A New Autofluoroscopic Camera[1,2,3]

William H. Beierwaltes, M.D., Gordon M. Brown, M.S.,
Lawrence W. Jones, Ph.D., and F. Deaver Thomas, M.D.

Ann Arbor, Michigan

INTRODUCTION

The ideal properties of a scintillation camera system for nuclear medicine would be: 1) 100% efficiency in detecting photons (X-rays or gamma-rays) entering its aperture, together with energy resolution or discrimination; 2) spatial resolution limited only by the source; 3) an effective solid angle approaching 4π radians to subtend as large a flux as possible of the available radiation; and 4) a field of view potentially as large as the patient. Obviously, no available instrument meets these criteria and indeed, they are in a sense mutually exclusive; for example, a large detector solid angle acceptance would sacrifice spatial resolution away from a shallow focal plane as a consequence of the constraints of geometrical optics. The camera systems previously described (1-10) all are limited by practical considerations far short of these ideal objectives. We believe that the new system described below may be a closer approach to these objectives. Essentially, the system consists of a NaI crystal to convert gamma rays to give rise to visible light quanta, which are then focused by a lens onto the photocathode of a 3-stage RCA image intensifier. The image intensifier amplifies the light from each scintillation pulse in the NaI crystal to a level where it can be recorded on film.

DESCRIPTION OF THE AUTOFLUOROSCOPIC CAMERA

Fig. 1 is a diagram of the autofluoroscopic camera, and Fig. 2 is a photograph of the completed prototype camera and mechanical hoist.

1. COLLIMATORS

Both pinhole and multichannel collimators are presently used with the camera. Figure 3 shows a cross sectional view of the pinhole collimator. It consists of a 2″ thick lead cylinder with a double 101° apex conic section removed from the center. The central section, which contains the pinhole aperture, is removable and interchangeable. Four mm and 10 mm apertures are presently used. The lead shield is held in an aluminum container which positions the pinhole 3.67″ (9.32 cm) in front of the scintillation crystal. The geometrical efficiencies at unity magnification are 7.2 x 10^{-4} and 1.15 x 10^{-4} for the 10 mm and 4 mm diameter pinholes, respectively, where the geometrical efficiency is defined as $\dfrac{\text{solid angle}}{4\pi}$.

The pinhole provides an inverted gamma ray image and is most useful when objects are imaged at magnifications different from unity or when the object must be spaced some distance from the detector (e.g., deep organs). Sensitivity is inversely proportional to the square of the distance from the aperture.

Two multichannel lead collimators have been constructed which are interchangeable with the pinhole collimator assembly (Fig. 4). The fine resolution,
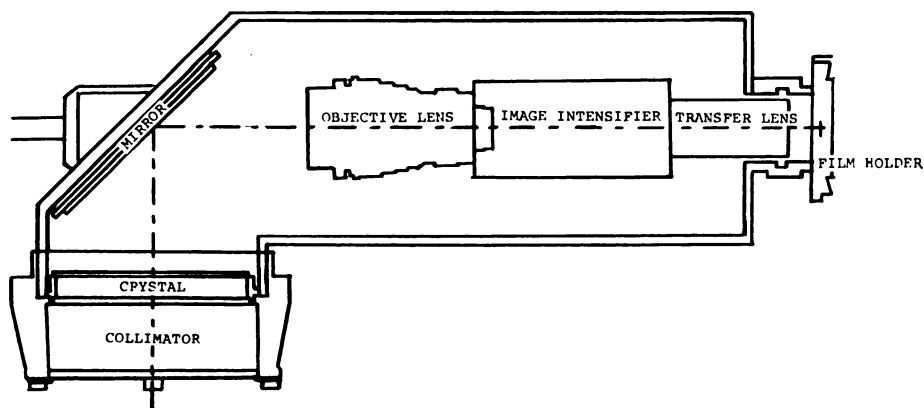

Fig. 1. Diagram of the autofluoroscope camera.

low efficiency collimator is 3" in height and 9.5" in overall diameter, has square apertures .033" in diameter, with septa .010" thick. The geometrical efficiency for objects placed at the surface is 1.62×10^{-5} and the clear area is 59%. There are over 38,000 parallel channels. The coarse collimator has the same overall dimensions and septa thickness, but the apertures are .109" in diameter. It has over 3600 parallel channels and its efficiency for objects placed at the surface is 7.8×10^{-5} and the clear area is 61.4%. These collimators are constructed from lead strips which were formed in a right triangle pattern with dies, glued together, cut in circular form and finally placed in an aluminum frame for protection. The detector side of the multichannel collimator is located 0.395" from the scintillation crystal.

The multichannel collimators are most useful for viewing large organs at unity magnification with the best compromise between sensitivity and resolution. The resolution decreases with increasing distance from the multichannel collimators; however, the efficiency as defined above is nearly constant.

2. IMAGE DETECTOR

The image detector consists of a thick scintillation single crystal, a fast objective lens, a high gain optical image intensifier, and a fast photographic recording system.
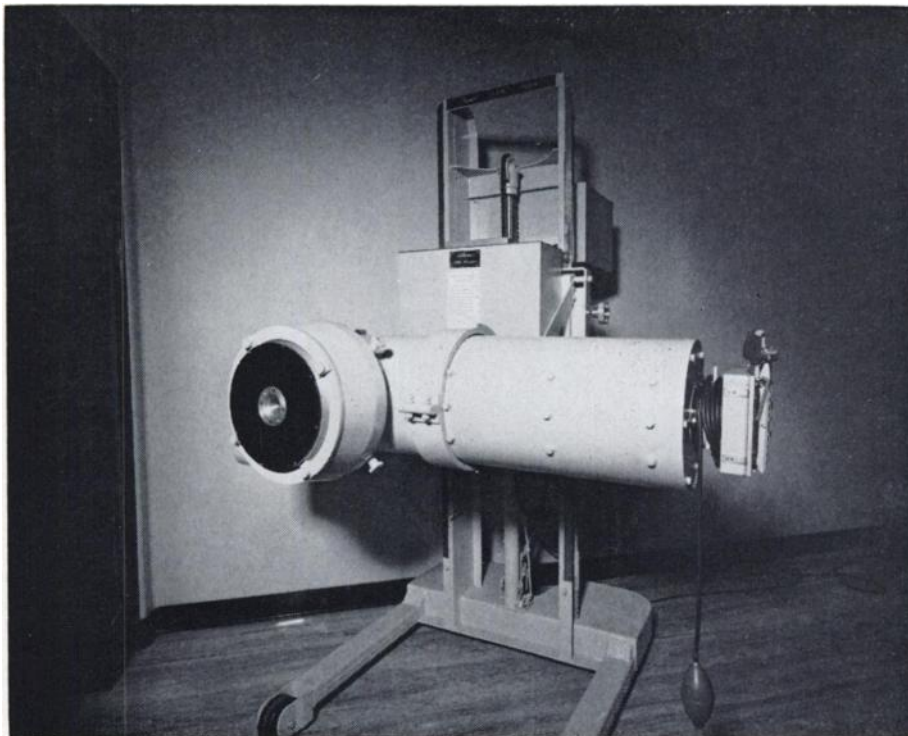

Fig. 2. Photograph of the completed prototype camera and mechanical hoist.
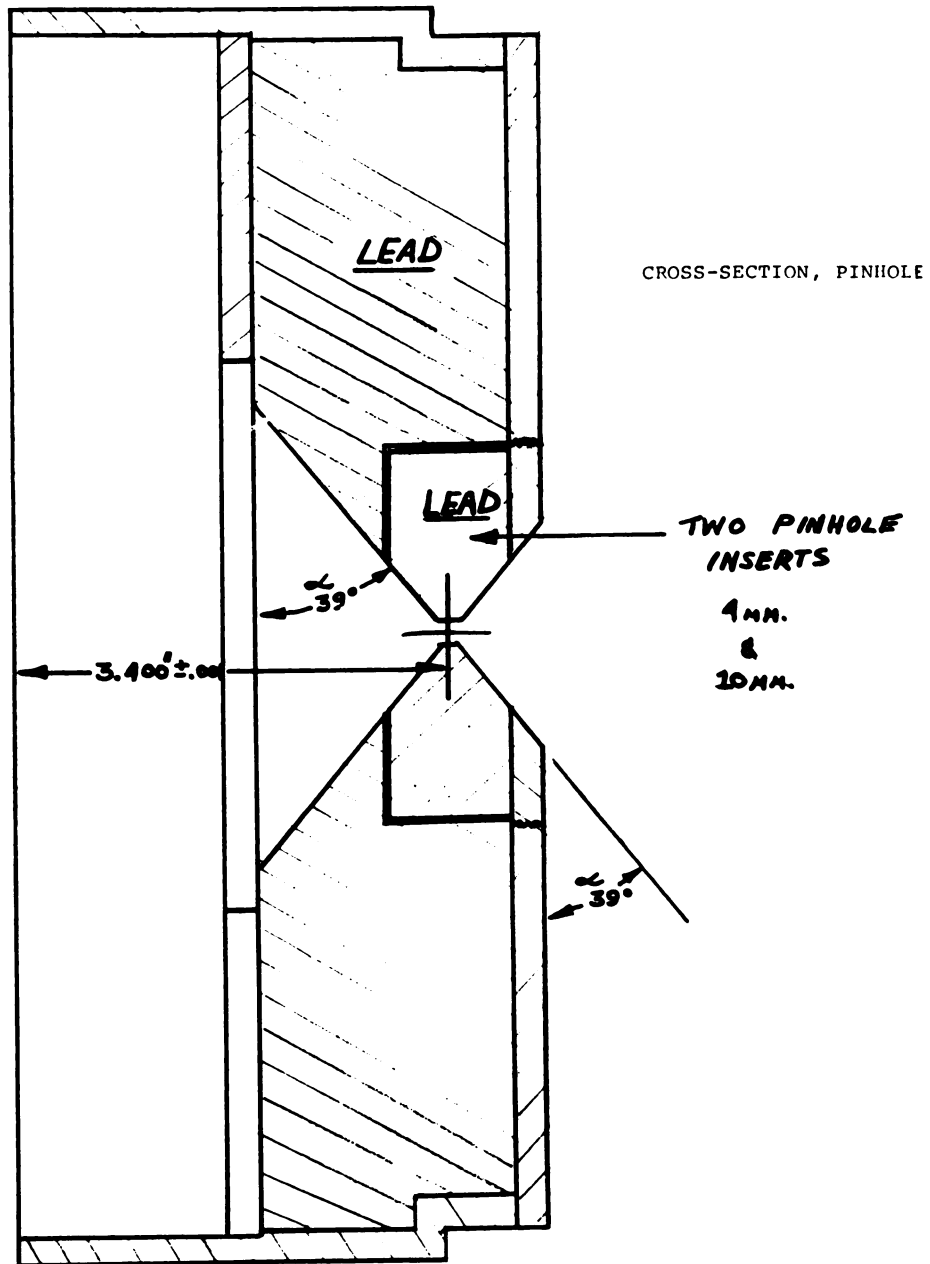
CROSS-SECTION, PINHOLE

LEAD

LEAD

TWO PINHOLE
INSERTS

4 MM.
&
10 MM.

39°

3.400' ±.00

39°

Fig. 3. Cross-sectioned view of the pinhole collimator, 2″ × 9.5″ with interchangeable pinholes 4 mm and 10 mm in diameter.

NaI CRYSTAL. Gamma rays are imaged by the collimators onto a 1″ thick, 9″ diameter NaI(Tl) scintillation crystal which converts interacting gammas into visible light. The crystal is optically coupled to the mirrored side of a ⅛″ thick Beryllium gamma ray entrance window. The exit window is a ¼″ thick plate glass optically coupled to the other side of the crystal. This assembly is hermetically sealed in an aluminum shell.

MIRROR AND LENS. The scintillation light is deflected 90° by a front-surface mirror and focused onto the photocathode of an image intensifier by a fast objective lens system. The objective lens consists of a f/0.87, 76 mm F.L. Super Farron coupled front-to-front with an f/4.5 18″ F.L. lens. The optical minification factor is 6:1, the effective f/number is 0.75 and the transmission is .36 for NaI(Tl) light.

IMAGE INTENSIFIER. The image intensifier is a 3-stage, cascaded, magnetically focused RCA C70021T which has a 38 mm diameter S-20 input photocathode and a 38 mm diameter P-11 output phosphor. Performance data for this tube are:

1. First photocathode radiant sensitivity: 77ma/watt
2. First photocathode quantum efficiency for NaI(Tl) light: 0.21
3. Radiant Power Conversion Gain: 2.5×10^5
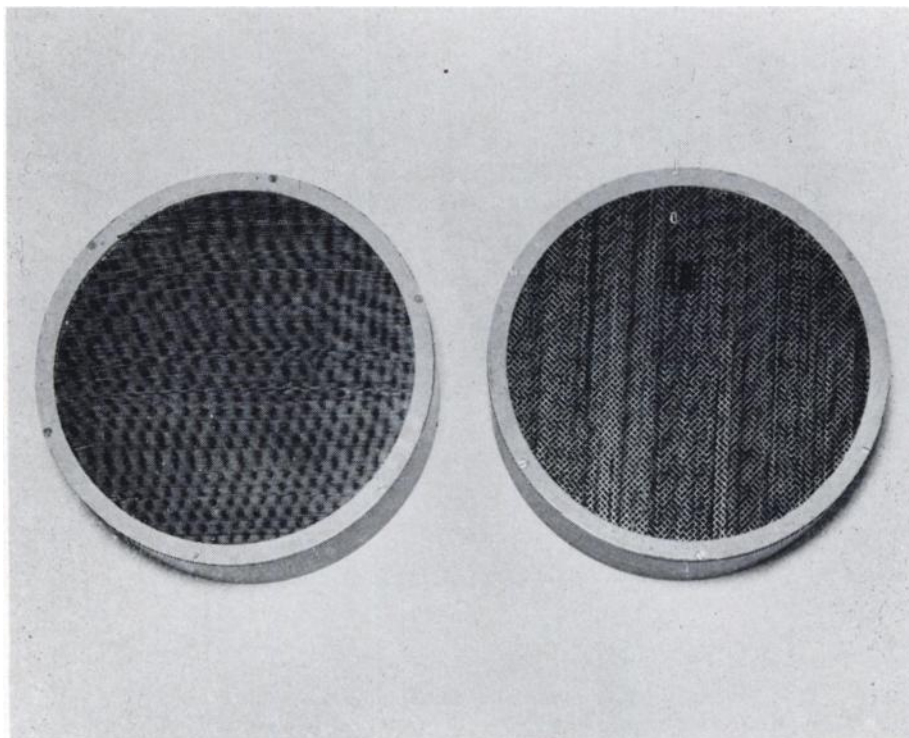
Fig. 4. Photograph of the two multichannel collimators.

a. Fine collimator. 3″ × 9.5″ overall with square apertures .033″ in diameter, with septa .01″ thick, 38,000 parallel channels.
b. Coarse collimator. Square apertures .109″ in diameter, 3,600 parallel channels.

4. Input equivalent of Screen Background: 3.7×10^{-4} x/cm^2 at 23° C
5. Resolution: Center, 18 lp/mm; edge, 14 lp/mm
6. Operating Voltage: 28.8 KV

TRANSFER LENS AND POLAROID FILM. The intensifier output is imaged onto 4″ × 5″ Polaroid film with an f/0.8, 38 mm, 1:1 transfer lens.

DETECTION EFFICIENCY AND INHERENT RESOLUTION OF THE IMAGE DETECTOR

The detection efficiency of the image detector is limited by (1) the scintillation crystal thickness and (2) the average number of photoelectrons per gamma ray absorption occurring in the primary photocathode of the image intensifier. The former limits the absorption efficiency at high gamma energies and the latter limits the sensitivity at the lower gamma energies.
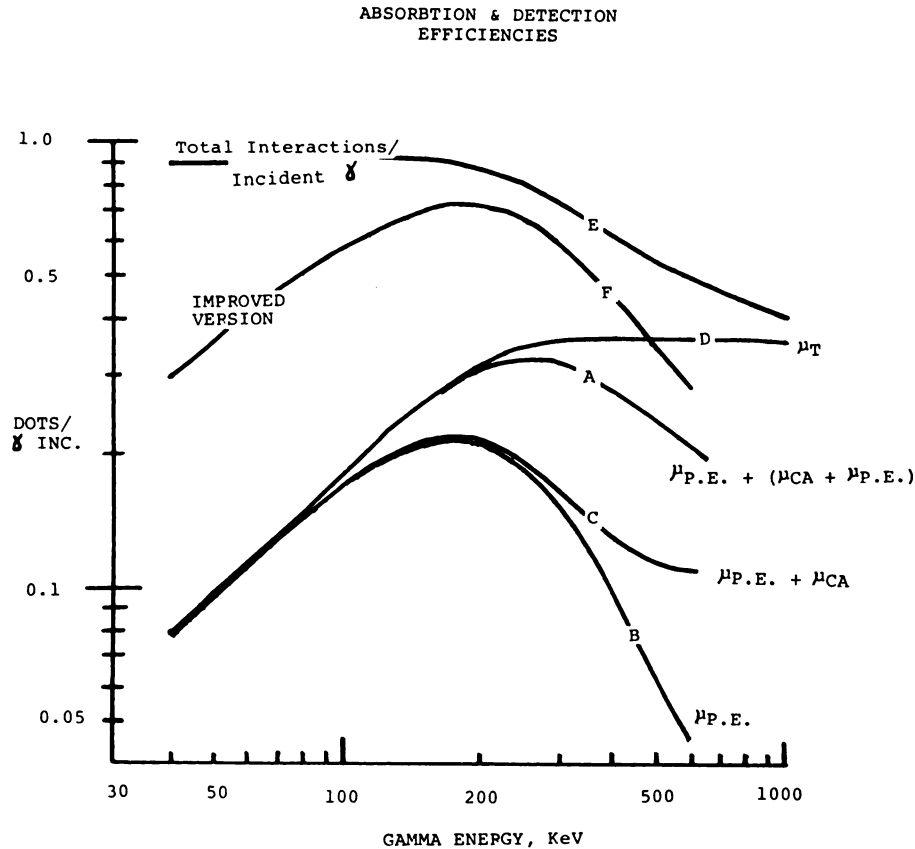

ABSORBTION & DETECTION
EFFICIENCIES

GAMMA ENERGY, KeV

Fig. 5. Calculation of absorption and detection efficiency (dots per indicent gamma). Curve A—for the present camera; curve B—for photoelectric absorption only; curve C—for photoelectric plus primary compton absorption; curve D—total absorption assuming all incident energy is deposited; curve E—total number of interactions per incident gamma; curve F—calculated detection efficiency of an improved detector where the lens efficiency is increased by 3 (Fresnel lens) and the photocathode quantum efficiency is increased by 1.5 (Bi-Alkali photocathode).

Fig. 6. Initial image at room temperature of standard thyroid phantom containing 10 mCi of ^{99m}Tc with coarse multichannel collimator, at a distance of 4 cm, 30 sec exposure time. Concentration of radioactivity in phantom ranged from 60 μCi/cm^2 to 30 μCi/cm^2.
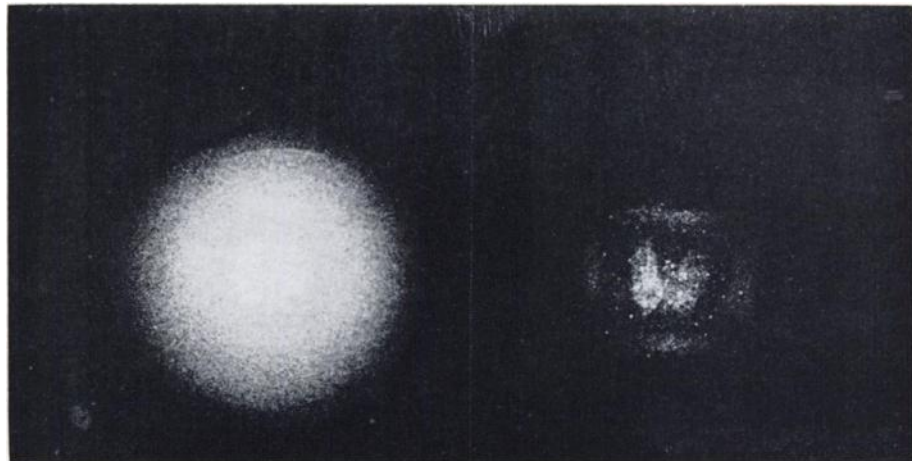
Fig. 7. Effect of cooling first photocathode with dry nitrogen (from 75° to 0° F) on thermo-ionic noise. The signal-to-noise ratio was increased by a factor of 100. Fine honey-comb collimator.

The scintillator thickness is necessarily a trade off between absorption efficiency and resolution limits introduced by Compton scattering and depth of field requirements on the objective lens. The photon collection efficiency of the objective lens ($\sim 3.24 \times 10^{-4}$), the quantum efficiency of the primary photocathode of the intensifier (~ 0.21) and the light conversion efficiency of the NaI(Tl) crystal (~ 30 ev/hγ) determine the average number of photoelectrons per gamma ray absorption. Since the emission of photoelectrons is essentially Poissonian, the average number of photoelectrons per absorption determines the probability that one or more photoelectrons will be emitted for a given event. Measurements demonstrate that each electron emitted from the primary photocathode creates enough light to be imaged onto Polaroid 57 film. Experiments were performed to measure the detection efficiency by counting the recorded dots on film from a known source and with the use of a multiplier phototube and pulse height analyzer looking at the output of the intensifier. Figure 5 presents the calculated detection efficiency (Dots per Incident Gamma) for the present detector (curve A). This includes the Beryllium window transmission, the total number of photoelectric and Compton plus photoelectric events and the probability that one or more photoelectrons are emitted per event, all as a function of gamma ray energy. Also shown are similar curves for photoelectric absorption only (curve B), photoelectric plus primary Compton absorption (curve C), total absorption assuming all incident energy is deposited (curve D) and the total number of interactions per incident gamma (curve E). Finally, curve F shows the detection efficiency of an improved detector (similar to curve A) where the lens efficiency is increased by 3 and the photocathode quantum efficiency is increased by 1.5. The use of a Fresnel lens and a Bi-Alkali photocathode can provide these improvements.

The inherent resolution of the image detector is limited by: 1) the 2″ depth of field imposed on the fast objective lens, and 2) multiple scattering within the scintillator. When multichannel collimators are used, penetration of the septa limits the resolution. Also, due to the large crystal thickness, oblique rays, which are incident at the edge of the field of view limit the resolution. Calculations indicate that the radius of confusion introduced by C above is about 1.4 to 1.5 mm. It is estimated that at 360 KeV, about 20% of the total absorption events in this crystal fall 3 mm or more from the primary events, as a result of the second interaction of Compton scattered gammas.

SENSITIVITY OF THE IMAGE DETECTOR

One of the major problems with this image detector is the primary photocathode noise. This noise limits integration time and increases the source strength requirements. At room temperature the present device is not suitable for *in vivo* studies on humans, since higher than normal radioactivities are required. A thyroid phantom[1] was loaded with 10mCi of ^{99m}Tc to provide minimal signal-to-

---

[1]Picker Nuclear thyroid phantom. Each thyroid "lobe" = 6 cm × 2.2 cm. Each pole has a "hole" 6-12 mm in diameter, with 20 ml in one lobe and 10 ml in the opposite lobe.

noise ratios with a 4 mm diameter pinhole collimator imaging 1:1. This corresponded to ~60 μCi/cm^2 in the most active part of the phantom and 30 μCi/cm^2 in the least active part. At this level of activity 12 mm and 6 mm diameter defects were observed at a distance of 4 cm with an exposure time of 30 sec, as shown in Figure 6.

Dry nitrogen was cooled in a heat exchanger and introduced into the photocathode cavity to reduce the photocathode temperature.

Figure 7 shows the effect of cooling the first photocathode with dry nitrogen (from 75° to 0° F) on thermal noise. The signal-to-noise ratio was increased by a factor of 25 by reduction of thermal noise by cooling.[2]

---

[2]Source was 125 μCi ^{125}I in the Picker Phantom, fine collimator ⅛" thick, source at surface of collimator.

PHOTOCATHODE OUTPUT
LUMINANCE
(Foot Lamberts)

PHOTOCATHODE LUMINANCE
vs.
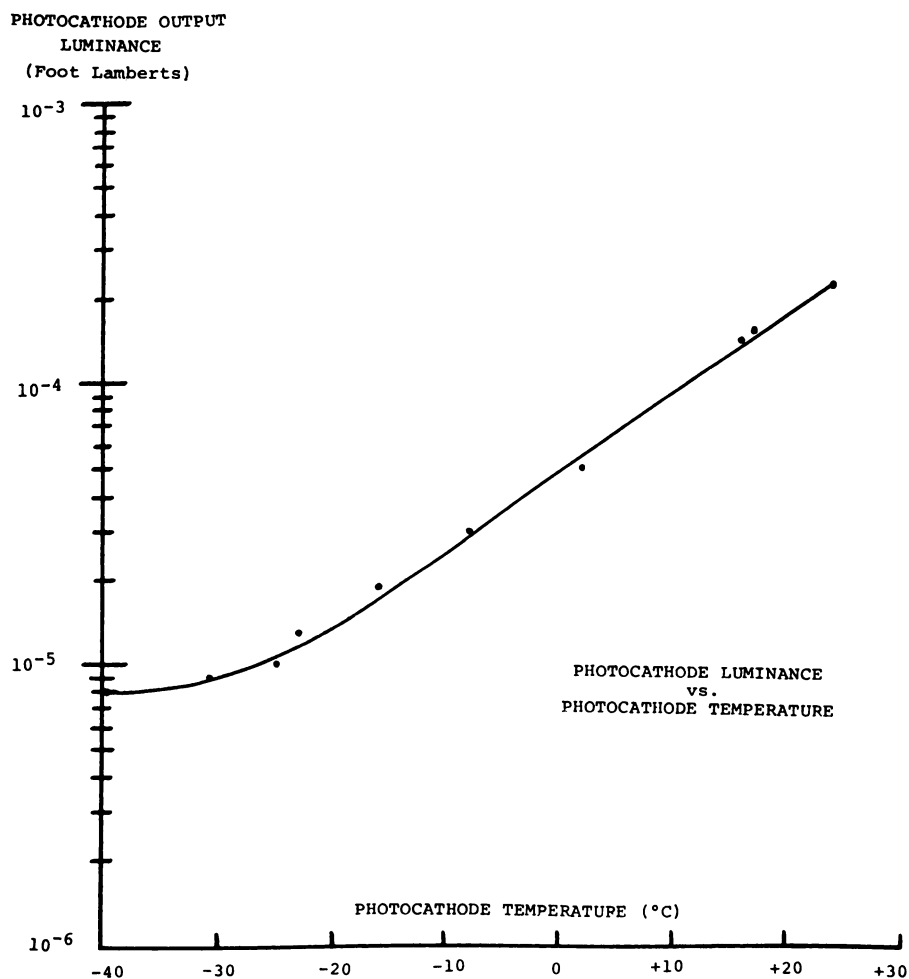PHOTOCATHODE TEMPERATURE

PHOTOCATHODE TEMPERATURE (°C)

Fig. 8. Plot of intensifier output luminance as a function of primary photocathode temperature.

Figure 8 shows a plot of the intensifier output luminance as a function of primary photocathode temperature.

Figure 9 presents the image produced of the same standard thyroid phantom containing 100 μCi of ^{99m}Tc with an exposure time of 10 sec, using the 4 mm channel collimator, at a distance of 4 cm at room temperature. Although the phantom is faintly visualized to the right of the cluster of ion spots, it is obvious that it would not be visualized if the ion spots were superimposed on the image.

Based on the original ^{99m}Tc phantom data taken with the cathode at room temperature, a reduction of 25 in thermal noise should allow useful viewing below 1.5-3.0 μCi/cm^2 with a 4 mm diameter pinhole imaging 1:1, providing that "ion spotting" is significantly reducible. To image 1 μCi/cc might be a reasonable "clinical" goal.

Figure 10 shows the calculated collimator efficiencies for a 4 mm pinhole imaging 1:2 and the 0.109″ × 3″ multichannel collimator in units of recordable dots/min/μCi, as well as the three other collimators presently being used.

Initially, another source of noise, "ion spots," remained essentially constant at 1.5 per sec over the entire sensitive area of the tube. However, after about 20 hr of operation, the number of "ion spots" increased to about 150 per sec at
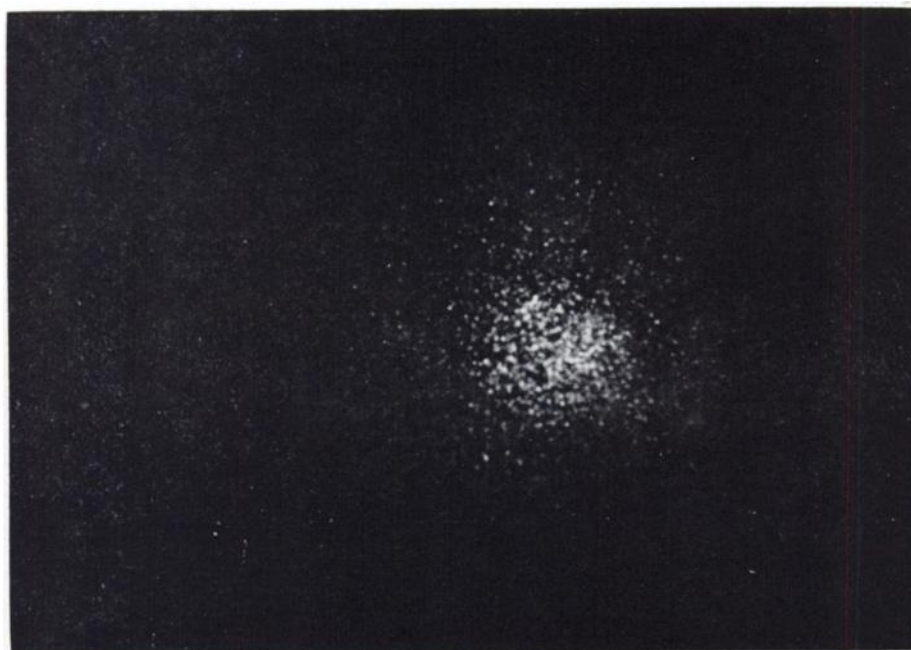

Fig. 9. Image produced of the same thyroid phantom shown in Fig. 7 containing 100 μCi of ^{99m}Tc with an exposure time of 6 minutes using a 4 mm channel collimator at a distance of 4 cm at room temperature. Although the phantom is faintly visualized to the right of the cluster of ion spots, it is obvious that it would not be visualized if the ion spots were superimposed on the image.

room temperature and appeared on film as bright spots covering the central third of the sensitive area. These new "ion spots" were found to decrease with temperature, but were never reduced to less than four to five times the original level. Needless to say, these "ion spots" hindered further phantom and *in vivo* studies. An increase in ion spotting was also observed when a small area signal was intro-
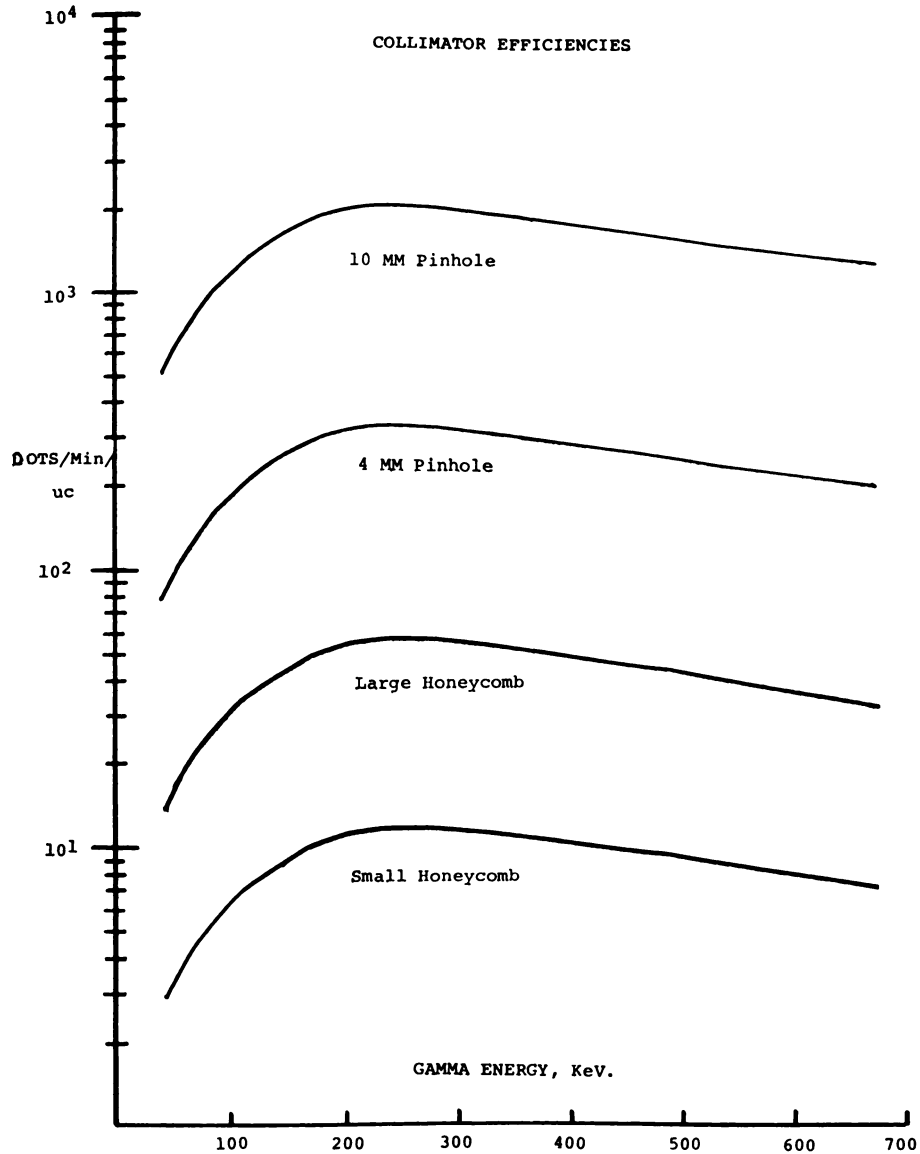

Fig. 10. Calculated collimator efficiencies for the 10 and 4 mm pinhole collimators imaging 1:2, and the coarse and fine multichannel collimators in units of recordable dots/ min/μCi.

duced. Ion spots seem to be a highly variable phenomenon in image tubes, with different tubes of the same type as well as the same tube at different times showing a very different level of ion spot noise.

DISCUSSION

Present utility of camera. Unfortunately this camera was not tested adequately with image phantoms or with patients with conventional doses of various types of radionuclides used in clinical Nuclear Medicine, while the camera was at its best performance level before the number of ion spots increased again with 20 hr of use. The phantom image shown in Fig. 9 above suggests, however, that further reduction in ion spotting would be desirable to image usual concentrations (10 μC rather than 100 μC) of radionuclides optimally *in vivo*.

Expectation for utility with improvements. The calculations presented in Fig. 5f, however, lead us to believe that with the use of a different lens and image intensifier, this camera will image satisfactorily at the radionuclide tissue concentrations usually present in clinical Nuclear Medicine diagnostic tests.

Pulse height resolution, noise reduction and positron annihilation detection might well be achieved through gating, either gating the last stage of this tube, or through a subsequent separate switch tube.

REFERENCES

1. ANGER, H. O.: Scintillation Camera with Multichannel Collimators. *J. Nucl. Med.,* 5:515, 1964.

2. ANGER, H. O.: Scintillation Camera with 11-inch Crystal. UCRL-11184, p. 69, 1963.

3. ANGER, H. O., AND DAVIS, D. H.: Gamma-ray-Detection Efficiency and Image Resolution in Sodium Iodide. UCRL-11184, p. 86, 1963.

4. ANGER, H. O.: Scintillation Camera Image Recording. UCRL-11336, p. 52, 1964.

5. BENDER, M. A.: The Digital Autofluoroscope. In: Medical Radioisotope Scanning: Proceedings of the Symposium on Medical Radioisotope Scanning, International Atomic Energy Agency in Athens, April 20-24, 1964. Vienna, International Atomic Energy Agency, Vol. 1:391, 1964.

6. GROSS, W., SCHLESINGER, E. B., AND DeBOVES, S.: A Scintillation Camera for Kinetic Studies of the Distribution of Radioactive Nuclides in the Brain. In: Medical Radioisotope Scanning: Proceedings of the Symposium on Medical Radioisotope Scanning, International Atomic Energy Agency in Athens, April 20-24, 1964. Vienna, International Atomic Energy Agency, Vol. 1:401, 1964.

7. KELLERSHOHN, C., AND PELLERIN, P.: Sur la Possibilite d'Utiliser un Tube Samplificateur d'Image pour Mettre en Evidence la Localisation et la Distribution d'un Corps Radioactiff. *C. R. Soc. Biol.* 149:533, 1955.

8. TER-POGOSSIAN, M. M., AND EICHLING, J. O.: Autofluorography with an X-ray Image Amplifier. In: Medical Radioisotope Scanning: Proceedings of the Symposium on Medical Radioisotope Scanning, International Atomic Energy Agency in Athens, April 20-24, 1964. Vienna, International Atomic Energy Agency, Vol. 1:411, 1964.

9. SLARK, N. A., AND WOOLGAR, A. J.: Transmission Secondary Emission Image Intensifiers. I.R.E. Trans. *Nuc. Sci.* NS9:115, June, 1962.

10. DUNHAM, CHARLES L.: Detectors in Biology and Medicine. In: Tenth Scintillation and Semiconductor Counter Symposium. IEEE Trans. on Nuclear Science NS-13, No. 3:9, 1966.